

Article

Influence of Proton Irradiation Energy on Gate–Channel Low-Field Electron Mobility in AlGa_N/Ga_N HEMTs

Qizheng Ji ^{1,2}, Jun Liu ³, Ming Yang ⁴, Xiaofeng Hu ¹, Guangfu Wang ⁵, Menglin Qiu ⁵ and Shanghe Liu ^{1,*}

¹ National Key Laboratory on Electromagnetic Environment Effects, Army Engineering University, Shijiazhuang Campus, Shijiazhuang 050003, China

² Beijing Institute of Spacecraft Environment Engineering, Beijing 100094, China

³ School of Electronics & Information Engineering, Nanjing University of Information Science & Technology, Nanjing 210044, China

⁴ Beijing Orient Institute of Measurement and Test, Beijing 100094, China

⁵ Key Laboratory of Beam Technology of Ministry of Education, College of Nuclear Science and Technology, Beijing Normal University, Beijing 100875, China

* Correspondence: liu_sh_h@163.com

Abstract: AlGa_N/Ga_N high-electron-mobility transistors (HEMTs) with two different gate–drain distances (30 μm and 10 μm) were exposed to 1 MeV, 0.6 MeV, and 0.4 MeV protons at a fluence of $2.16 \times 10^{12} \text{ cm}^{-2}$. The gate–channel electron density and low-field mobility were obtained by measuring the capacitance–voltage characteristics and current–voltage characteristics. After proton irradiation, the gate–channel low-field electron mobility of the AlGa_N/Ga_N HEMT with a 30 μm gate–drain distance increases and that with a 10 μm gate–drain distance decreases. It is studied and found that the mobility behavior is related to the polarization Coulomb field scattering, and the proton irradiation influences the intensity of the polarization Coulomb field scattering by changing the polarization/strain distribution in the barrier layer. The different gate–drain distances correspond to different variation trends of scattering intensity. The effect of 1 MeV protons on the barrier layer is smaller compared with 0.6 MeV and 0.4 MeV protons, so the mobility variation is smaller.

Keywords: AlGa_N/Ga_N HEMTs; proton; polarization; scattering



Citation: Ji, Q.; Liu, J.; Yang, M.; Hu, X.; Wang, G.; Qiu, M.; Liu, S.

Influence of Proton Irradiation Energy on Gate–Channel Low-Field Electron Mobility in AlGa_N/Ga_N HEMTs. *Electronics* **2023**, *12*, 1473. <https://doi.org/10.3390/electronics12061473>

Academic Editor: Francesco Giuseppe Della Corte

Received: 8 February 2023

Revised: 10 March 2023

Accepted: 18 March 2023

Published: 20 March 2023



Copyright: © 2023 by the authors. Licensee MDPI, Basel, Switzerland. This article is an open access article distributed under the terms and conditions of the Creative Commons Attribution (CC BY) license (<https://creativecommons.org/licenses/by/4.0/>).

1. Introduction

AlGa_N/Ga_N high-electron-mobility transistors (HEMTs) have the advantages of high breakdown voltage, high electron mobility, and high power density. They can work stably under harsh environments such as high temperature and high radiation due to the large band gap. Therefore, AlGa_N/Ga_N HEMTs have broad application prospects in important fields such as radar communication, aerospace, and nuclear reactors [1–6].

Compared with Si- and GaAs-based devices, the better radiation resistance of AlGa_N/Ga_N HEMTs has been proven theoretically [7,8]. However, during the growth process of the epitaxial layers, the lattice mismatch and thermal mismatch between the epitaxial layers induce a high density of defects [9,10]. It is a considerable challenge to the radiation resistance of AlGa_N/Ga_N HEMTs in practical applications. In addition, as one of the main particles causing the degradation of the device performance in the radiation environment, the study of the proton irradiation of AlGa_N/Ga_N HEMTs has received much attention. Hu et al. reported that the output characteristics and the transfer characteristics of the AlGa_N/Ga_N HEMTs degraded slightly at the 15, 40, and 105 MeV proton irradiations, but the drain current and transconductance decreased by 10% and 6.1% for a 1.8 MeV fluence of 10^{12} cm^{-2} , respectively [11]. The degradation of AlGa_N/Ga_N HEMTs at different proton energies is consistent with the calculation of the non-ionizing energy loss. Kalavagunta et al. reported that the gate-lag of AlGa_N/Ga_N HEMTs increases with a fluence increasing (from $3 \times 10^{12} \text{ cm}^{-2}$ to $3 \times 10^{14} \text{ cm}^{-2}$) at a 1.8 MeV proton irradiation [12]. Lv et al. studied

the influence of 3 MeV protons on AlGaN/GaN HEMTs [13]. In addition, they observed that the drain saturation currents and maximum transconductance decreased by 20% and 5%, respectively. The degree of the threshold voltage shift increased with the proton fluence increasing. The density of vacancies at different proton fluences were calculated by using SRIM and adding the vacancies model into a Silvaco simulator. It is found that the result of the simulation is consistent with the experimental data and the Ga vacancies may be the main reason for the degradation of the AlGaN/GaN HEMTs' performance. Ives et al. studied the effects of displacement damage induced by protons on AlGaN/GaN HEMTs [14]. The threshold voltage has a negative shift at a fluence of 10^{13} cm^{-2} and a positive shift at a high fluence of 10^{14} cm^{-2} . It is attributed to the proton-induced donor defects (N vacancies) dominating at a low fluence and acceptor defects (Ga vacancies) dominating at a high fluence. Kim et al. studied the DC characteristic degradation of AlGaN/GaN HEMTs at the 0.5 MeV, 5 MeV, and 60 MeV proton irradiations, and the transfer characteristics at a 0.5 MeV proton irradiation has the most serious degradation. Moreover, the threshold voltage at the 0.5 MeV and 5 MeV proton irradiations has a positive shift, while the threshold voltage at a 60 MeV proton irradiation has a negative shift [15]. According to different scattering mechanisms, Tang et al. developed a model to simulate two-dimensional electron mobility at different proton energies and fluences at a low temperature [16]. It is found that the proton-induced ionized impurity scattering is the dominant factor in the degradation of electron mobility at a very low temperature ($<5 \text{ K}$). The theoretical model of the proton irradiation effects on the two-dimensional electron density of AlGaN/GaN HEMTs were developed in the subsequent work [17]. The decrease of the electron density is a result of two mechanisms: the Fermi level is affected by the Ga vacancies in the GaN cap layer and AlGaN barrier layer, and the Ga vacancies in the GaN cap layer traps two-dimensional electrons in the potential well. These studies all consider that the displacement effect caused by proton irradiation is the main reason for the change of the AlGaN/GaN HEMTs' performance. However, little attention has been paid to the proton influence on piezoelectric polarization.

For AlGaN/GaN HEMTs, the existence of two-dimensional electron gas (2DEG) in the channel depends on the spontaneous and piezoelectric polarization [18]. A change of the lattice structure, which is induced by the displacement effect, will inevitably affect the polarization charge distribution by changing the strain distribution. It has been proven that the polarization Coulomb field (PCF) scattering is a special and important scattering mechanism in AlGaN/GaN HEMTs, and the PCF scattering is directly related to the device size and polarization charge distribution at the AlGaN/GaN interface [19–23]. Therefore, proton irradiation will alter the electron mobility of AlGaN/GaN HEMTs and device performance through PCF scattering. Therefore, particular attention should be paid to the proton influence on PCF scattering.

In this paper, AlGaN/GaN HEMTs with two different gate–drain distances (30 μm and 10 μm) were prepared, which were irradiated with different proton energies (1 MeV, 0.6 MeV, and 0.4 MeV) at a fluence of $2.16 \times 10^{12} \text{ cm}^{-2}$. The capacitance–voltage (C–V) characteristics and current–voltage characteristics were measured before and after irradiation. The low-field electron mobility is extracted, the low-field electron mobility of the device with a 30 μm gate–drain distance gets increased, and that of the device with a 10 μm gate–drain distance gets decreased after proton irradiation. The degree of the low-field electron mobility variation decreases with the increase of proton energy. The proton irradiation effect on the two-dimensional electron transport properties is analyzed by using the theoretical model of PCF scattering related to the device size and polarization/strain distribution at the AlGaN/GaN interface.

2. Materials and Methods

Figure 1 shows the structure of AlGaN/GaN HEMTs in this study. The metal–organic chemical vapor deposition (MOCVD) was used to fabricate the AlGaN/GaN heterostruc-

ture material on Si substrate. The epitaxial layers are formed by 3.9 μm GaN buffer layer, 0.26 μm i-GaN layer, 27.5 nm $\text{Al}_{0.25}\text{Ga}_{0.75}\text{N}$ barrier layer, and 3.3 nm GaN cap layer.

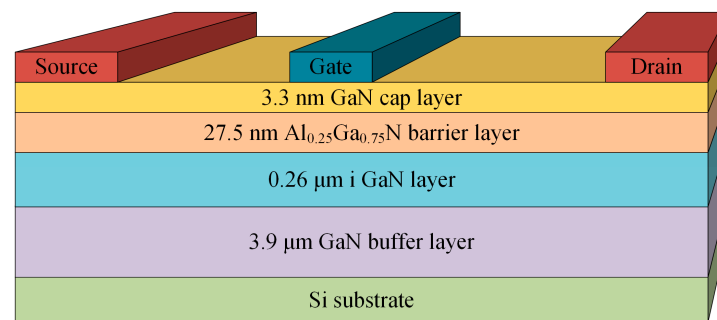


Figure 1. Device structure of AlGaN/GaN HEMTs.

Source and drain are both Ohmic contacts and gate is Schottky contact. Gate–source distance L_{GS} is 4 μm . Gate length L_G is 4 μm , and gate width W_G is 104 μm . The gate–drain distance L_{GD} are 30 μm and 10 μm , which are marked as Device 1 and Device 2, respectively.

Proton irradiation was performed in a proton accelerator with the device temperature controlled at room temperature during irradiation. Devices were irradiated with 1 MeV, 0.4 MeV, and 0.6 MeV protons at a fluence rate of $10^8 \text{ cm}^{-2}/\text{s}$. The proton irradiation lasted for 6 h, meaning a fluence of $2.16 \times 10^{12} \text{ cm}^{-2}$. The C – V characteristics and current–voltage characteristics were measured before and after proton irradiation.

3. Results and Discussion

Figure 2 shows the C – V curves of the AlGaN/GaN HEMTs measured at 1 MHz before and after proton irradiation. The C – V curve at 1 MHz reveals the information of 2DEG at the AlGaN/GaN interface. The gate–channel 2DEG electron density n_{2D} can be obtained by the following equation [24]:

$$n_{2D} = \int_{V_T}^{V_{GS}} C dV / (Me) \quad (1)$$

where C is the gate–source capacitance, V_T is the threshold voltage, V_{GS} is the gate–source voltage, M is the area of the gate Schottky contact, and e is the electron charge. V_T is obtained by differentiating the C – V curve. Before irradiation, the V_T values of Device 1 and Device 2 are both -4.95 V . After irradiation, the V_T values of Device 1 are -4.95 V (1 MeV proton energy), -4.9 V (0.6 MeV proton energy), and -4.85 V (0.4 MeV proton energy). The V_T values of Device 2 after irradiation are -4.95 V (1 MeV proton energy), -4.95 V (0.6 MeV proton energy), and -4.85 V (0.4 MeV proton energy). The shift of V_T is related to the electron density [25]. The obtained n_{2D} is shown in Figure 3. It is found that the n_{2D} of Device 1 and Device 2 decrease by different degrees after irradiation. Protons cause displacement damage at the AlGaN/GaN interface, which is the main reason for the decrease of the electron density [13]. The decrease in n_{2D} is the most obvious after a 0.4 MeV proton irradiation. With proton energy increasing, the degree of decrease in electron density gradually gets smaller. The decrease after a 1 MeV proton irradiation is the least. It explains that the degree of threshold voltage shift increases as proton energy decreases.

Figures 4 and 5 are the I_{DS} – V_{DS} curves of Device 1 and Device 2 before and after proton irradiation. I_{DS} and V_{DS} are the drain–source current and drain–source voltage, respectively. It is found that the I_{DS} of Device 1 increases and I_{DS} of Device 2 decreases after 0.4 MeV irradiation. With proton energy increasing, the difference in the I_{DS} between Device 1 and Device 2 is gradually disappearing. I_{DS} is dominated by both electron density and electron mobility. The electron density of Device 1 and Device 2 both decrease after irradiation (Figure 3), and it cannot explain the increase of I_{DS} in Device 1 (Figure 4c). Thus, the difference in the I_{DS} between Device 1 and Device 2 should be induced by electron

mobility. According to the $I_{DS}-V_{DS}$ curves, the gate-channel 2DEG electron mobility μ_n is obtained as follows [24,26–28]:

$$\mu_n = \frac{I_{DS}L_G}{en_{2D}W_G[V_{DS} - I_{DS}(R_d + R_s + 2R_c)]} \tag{2}$$

$$R_d = \frac{L_{GD}}{en_{2D0}\mu_{n0}W_G} \tag{3}$$

$$R_s = \frac{L_{GS}}{en_{2D0}\mu_{n0}W_G} \tag{4}$$

where R_d is the gate-drain access resistance, R_s is the gate-source access resistance, $R_c = 3.54 \Omega \cdot \text{mm}$ is the Ohmic contact resistance, which is obtained by the transmission line method (TLM), and n_{2D0} and μ_{n0} are the gate-channel 2DEG electron density and mobility corresponding to $V_{GS} = 0 \text{ V}$. The values of I_{DS} at $V_{DS} = 0.1 \text{ V}$ are adopted corresponding to the low-field region [27–29].

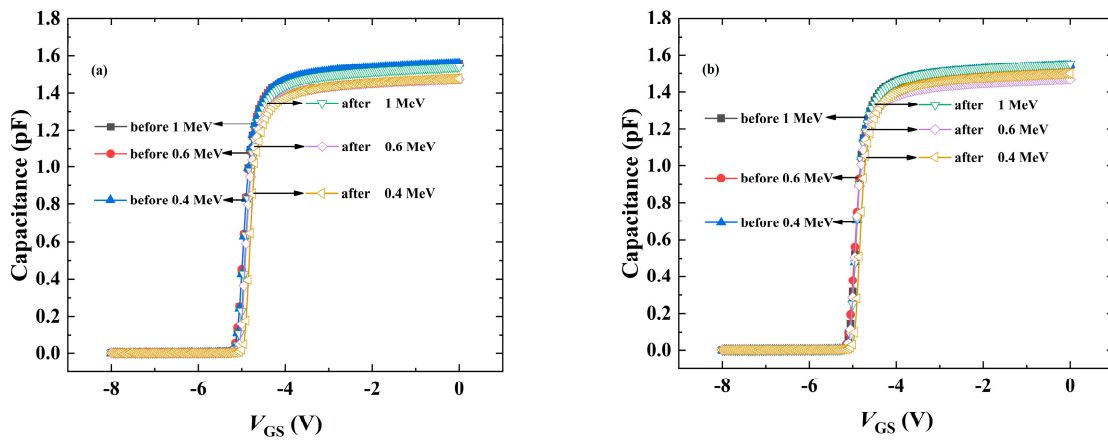


Figure 2. Measured C–V curves before and after proton irradiation for Device 1 (a) and Device 2 (b).

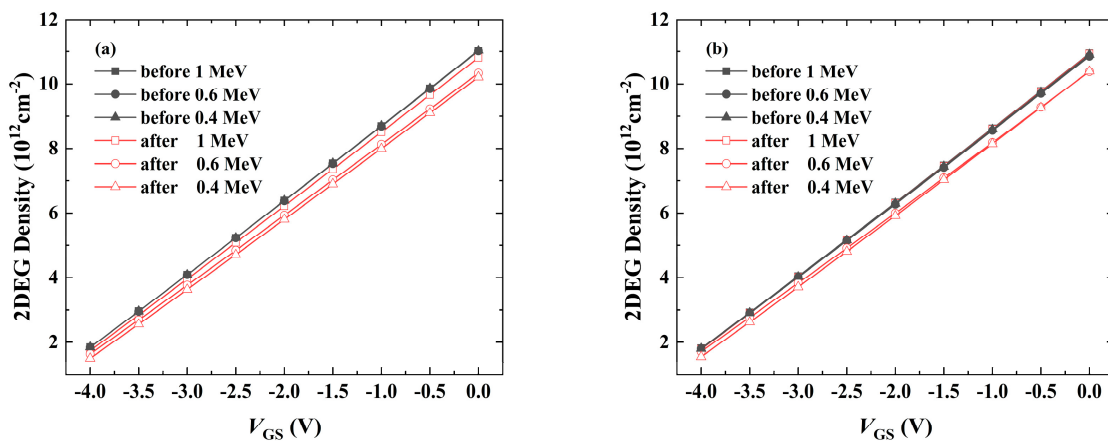


Figure 3. Gate-channel 2DEG electron density n_{2D} as a function of gate voltage for Device 1 (a) and Device 2 (b).

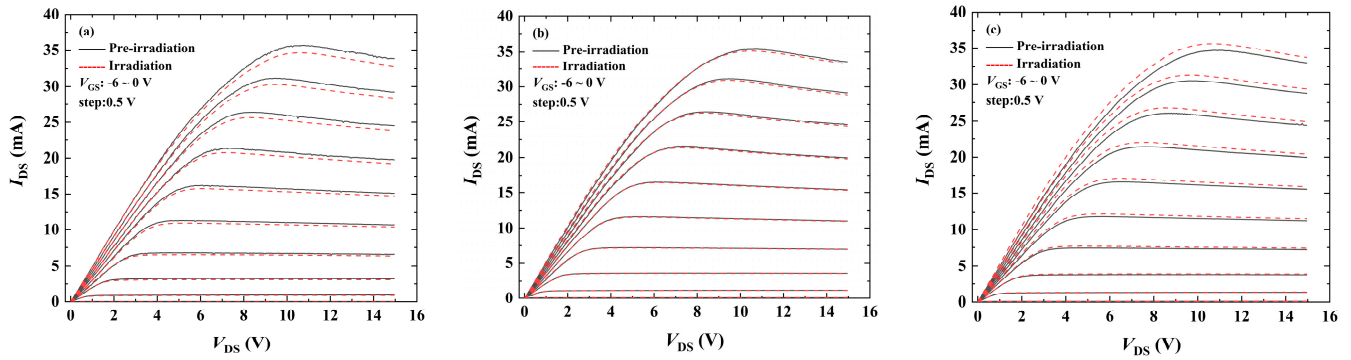


Figure 4. Measured I_{DS} – V_{DS} curves of Device 1 before (“Pre-irradiation”) and after (“Irradiation”) proton irradiation with 1 MeV (a), 0.6 MeV (b), and 0.4 MeV (c) proton energies.

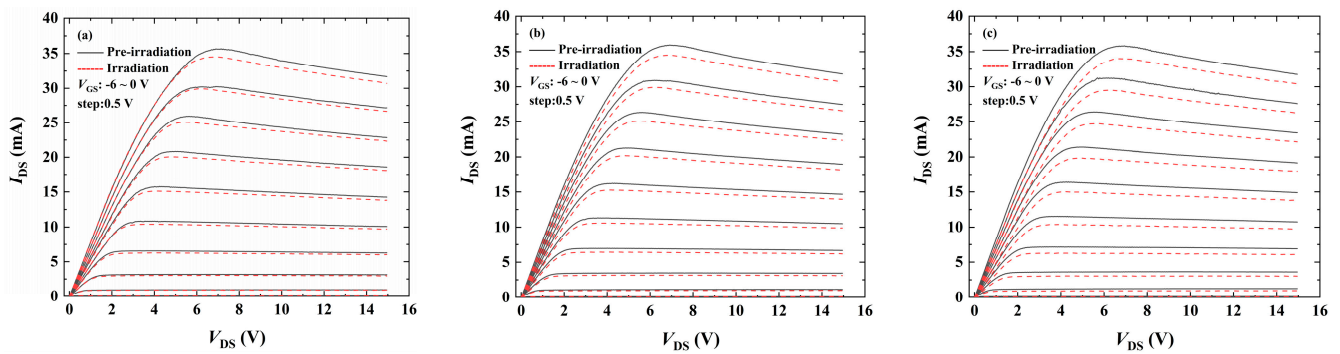


Figure 5. Measured I_{DS} – V_{DS} curves of Device 2 before (“Pre-irradiation”) and after (“Irradiation”) proton irradiation with 1 MeV (a), 0.6 MeV (b), and 0.4 MeV (c) proton energies.

Figures 6 and 7 show the μ_n of Device 1 and Device 2 before and after proton irradiation. In order to provide a clear comparison, the average change rates of μ_n for Device 1 and Device 2 under the 1 MeV, 0.6 MeV, and 0.4 MeV proton irradiations are given in Table 1. After a 0.4 MeV proton irradiation, the μ_n of Device 1 increases by 14.3% (Figure 6c) and that of Device 2 decreases by 15.0% (Figure 7c). As the proton energy increases, the magnitude of the μ_n variation for Device 1 and Device 2 gradually decrease. After a 1 MeV proton irradiation, there is a slight increase (+5.4%) in the μ_n of Device 1 (Figure 6a) and a slight decrease (−5.4%) in the μ_n of Device 2 (Figure 7a). It is found that the electron mobility varies differently between the devices with two different gate–drain distances and the magnitude of the variation decreases with the proton energy increasing. This μ_n behavior is explained as follows.

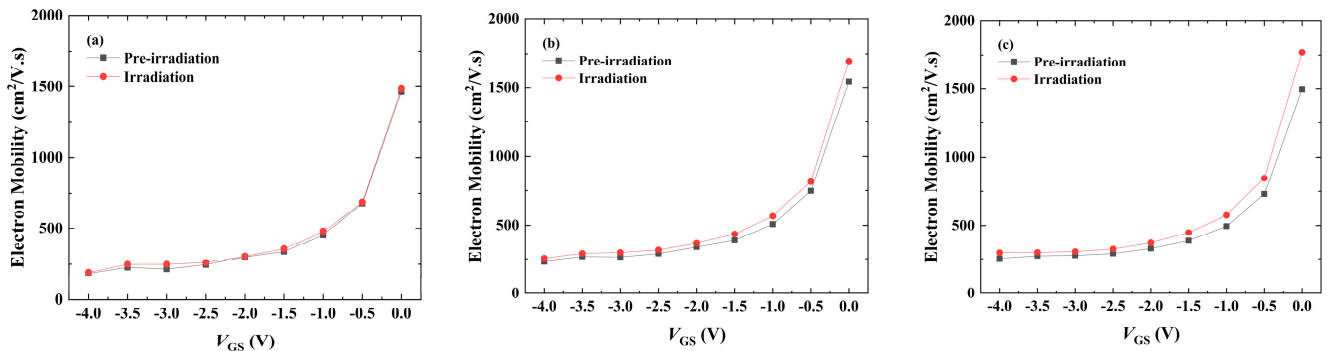


Figure 6. Gate–channel low-field electron mobility μ_n of Device 1 before (“Pre-irradiation”) and after (“Irradiation”) proton irradiation as a function of gate voltage with 1 MeV (a), 0.6 MeV (b), and 0.4 MeV (c) proton energies.

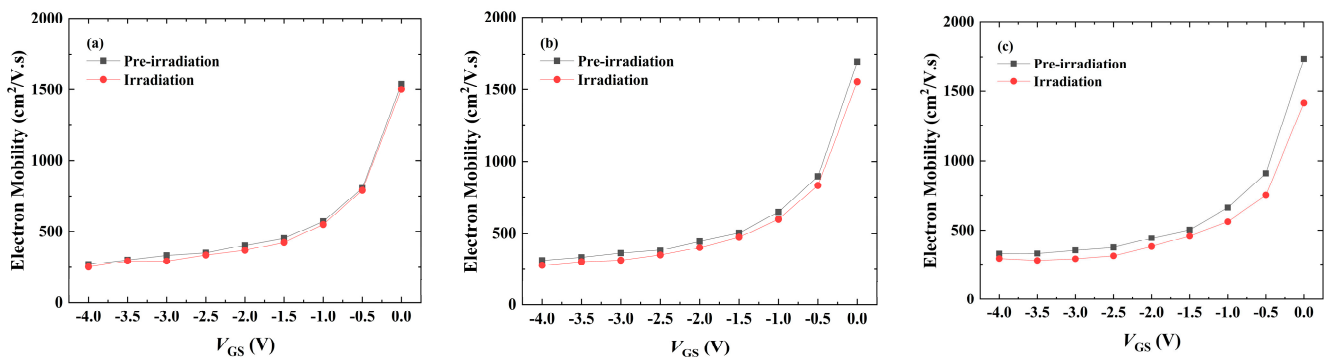


Figure 7. Gate–channel low-field electron mobility μ_n of Device 2 before (“Pre-irradiation”) and after (“Irradiation”) proton irradiation as a function of gate voltage with 1 MeV (a), 0.6 MeV (b), and 0.4 MeV (c) proton energies.

Table 1. Average change rate of μ_n for Device 1 and Device 2 with 1 MeV, 0.6 MeV, and 0.4 MeV protons.

Proton Energy (MeV)	Average Change Rate of μ_n for Device 1 (%)	Average Change Rate of μ_n for Device 2 (%)
1	+5.4	−5.4
0.6	+10.2	−9.0
0.4	+14.3	−15

In AlGa_N/Ga_N HEMTs, electron mobility is mainly determined by the polar optical phonon (POP) scattering, acoustic phonon (AP) scattering, interface roughness (IFR) scattering, dislocation (DIS) scattering, and PCF scattering [29–31]. The first four scattering mechanisms are determined by the inherent properties of the AlGa_N/Ga_N material and are not affected by the device size [20,31,32]. The devices in this study are fabricated on the same heterostructure material, so the first four scattering mechanisms of Device 1 are consistent with that of Device 2. Since the protons are uniformly irradiated over the devices, the variations of the inherent properties are the same for Device 1 and Device 2 under the same irradiation environment. For devices in the same proton irradiation environment, the variation of μ_n should be consistent under the influence of the first four scattering mechanisms after proton irradiation, which is inconsistent with the experimental results (Figures 6 and 7). Previous studies have reported that PCF scattering is closely related to device size [19–23,28,29]. Therefore, although μ_n is dominated by POP scattering at room temperature, the differences in μ_n behavior corresponding to the different L_{GD} (Figures 6 and 7) must be attributed to PCF scattering.

Before device fabrication, the polarization charges in the heterostructure material are uniformly distributed. The device fabrication processing (rapid thermal annealing) and gate bias cause the nonuniform distribution of polarization charges at the AlGa_N/Ga_N interface [24,29]. The PCF scattering of the AlGa_N/Ga_N HEMTs originates from the difference between the nonuniform polarization charges and the uniform polarization charges, which is defined as the additional polarization charges $\Delta\sigma$. Figure 8 is the $\Delta\sigma$ distribution diagram. The influence of the additional polarization charges near the Ohmic contact is negligible, considering that L_{GS} and L_{GD} are large enough and μ_n before irradiation is almost the same (Figures 6 and 7) [29]. Therefore, the distribution of $\Delta\sigma$ is mainly divided into two parts, as shown in Figure 8. In region I, which is influenced by the converse piezoelectric effect, the negative gate bias compresses the lattices and the polarization charges decrease, generating the negative additional polarization charges $\Delta\sigma_1$. Due to the lattice continuity, the compression of the lattices in region I causes the tensile strain of the adjacent lattices in region II and the polarization charges increase, generating the positive additional polarization charges $\Delta\sigma_2$ [18,28]. The tensile effect weakens with the distance increasing, so the additional polarization charges in region II are linearly distributed. In addition, although L_{GS} is different from L_{GD} , the interaction effect of region I is the same for both the gate–source region and gate–drain region, and the effect of protons on the

gate–source region and gate–drain region is also the same. For a clearer presentation and ease of understanding, the additional polarization charges of the gate–source region are treated the same as that of the gate–drain region. With this distribution of the additional polarization charge, the PCF scattering potential $V(x,y,z)$ generates the following [29]:

$$\begin{aligned}
 V(x,y,z) = & -\frac{e}{4\pi\epsilon_s} \int_{-L_{GS}-\frac{L_G}{2}}^{-\frac{L_G}{2}} dx' \int_0^{W_G} \frac{\Delta\sigma_2 \cdot (-x' - L_{GS} - L_G/2)}{L_{GS} \cdot \sqrt{(x-x')^2 + (y-y')^2 + z^2}} dy' \\
 & -\frac{e}{4\pi\epsilon_s} \int_{-\frac{L_G}{2}}^{\frac{L_G}{2}} dx' \int_0^{W_G} \frac{\Delta\sigma_1}{\sqrt{(x-x')^2 + (y-y')^2 + z^2}} dy' \\
 & -\frac{e}{4\pi\epsilon_s} \int_{\frac{L_G}{2}}^{L_{GD}+\frac{L_G}{2}} dx' \int_0^{W_G} \frac{\Delta\sigma_2 \cdot (x' - L_{GD} - L_G/2)}{L_{GD} \cdot \sqrt{(x-x')^2 + (y-y')^2 + z^2}} dy'
 \end{aligned} \tag{5}$$

where ϵ_s is the GaN dielectric constant. It is found from Equation (5) that the PCF scattering intensity is closely related to the device size and $\Delta\sigma$ distribution.

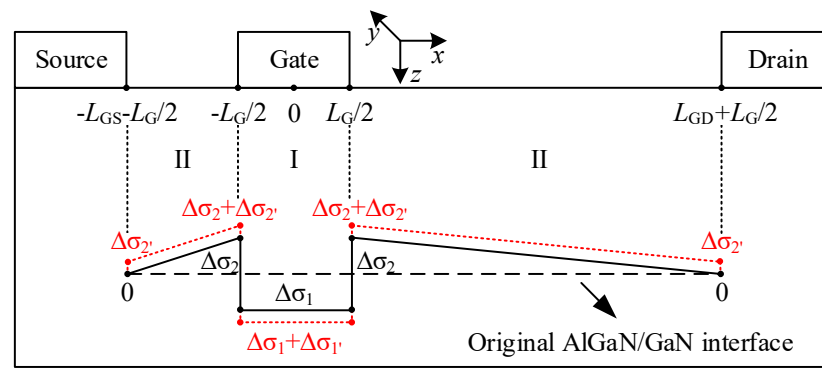


Figure 8. Distribution of additional polarization charges at AlGaIn/GaN interface.

Based on Figure 3, the level of the n_{2D} variation Δn_{2D} after proton irradiation at $V_{GS} = 0$ V as a function of proton energy is obtained and is shown in Figure 9. Since the 2DEG of the AlGaIn/GaN HEMTs is determined by the strain and polarization, the n_{2D} variation after proton irradiation indirectly reflects the lattice strain and polarization of region I, and the increase/decrease of the electron density corresponds to the enhanced/weakened tensile strain [18,33,34]. It is found from Figure 9 that the n_{2D} of both Device 1 and Device 2 decrease, and the Δn_{2D} of Device 1 is larger than that of Device 2. This means that the tensile strain in region I is weakened after proton irradiation. In addition, the weakening amplitude of Device 1 is greater than that of Device 2. A previous study has reported that the effects of protons on the AlGaIn/GaN heterostructure material are the ionization effect and displacement effect [35]. The ionization effect is the proton interaction with the lattice electrons, and the displacement effect is protons forcing atoms to leave the original lattice position [35]. The ionization effect will not change the lattice structure, so the change of the strain and polarization is caused by the displacement effect. Due to the same structure and size of the Schottky gates, at the same proton energy, the proton effect on region I should be the same for Device 1 and Device 2. Device 1 and Device 2 differ only in the gate–drain distance, so the variation of the tensile strain in region I must be attributed to the indirect effect of the adjacent region II. Since region I is covered by the gate metal, which has a blocking effect on protons, the proton irradiation effect of region I is different from that of region II. This makes the proton irradiation effect on the strain/polarization distribution of region I and region II different. Moreover, the PCF scattering is directly related to the nonuniform polarization charge distribution. Therefore, the main focus of this study is on the difference of the polarization distribution brought by proton irradiation for region I and region II. The enhancement of the tensile strain in region II can be inferred from the weakened tensile strain in region I. Compared with Device 2, the enhancement of the tensile strain in region II of Device 1 is greater, considering the greater weakening of

the tensile strain in region I. The positive additional polarization charges $\Delta\sigma_2$ is added to $\Delta\sigma_2$ due to the enhanced tensile strain in region II (Figure 8). In addition, since $\Delta\sigma$ is the additional polarization charges per unit area, and protons are uniformly irradiated on the devices, $\Delta\sigma_2$ is the same in Device 1 and Device 2. The enhanced tensile strain in region II weakens the tensile strain in region I because of the lattice continuity, generating the extra negative additional polarization charges $\Delta\sigma_1'$ (Figure 8). According to Equation (5), the additional polarization charges in region I and region II have an offsetting effect, which affects the PCF scattering potential. A larger L_{GD} will correspond to a stronger offsetting effect. For Device 1, the offset of $\Delta\sigma_2 + \Delta\sigma_1'$ to $\Delta\sigma_1 + \Delta\sigma_1'$ is stronger due to the larger L_{GD} . According to Equation (5), the PCF scattering potential becomes weaker and μ_n gets larger after proton irradiation (Figure 6). For Device 2, L_{GD} is smaller, which corresponds to a smaller integration interval of the last term in Equation (5). In addition, the offset of $\Delta\sigma_2 + \Delta\sigma_1'$ to $\Delta\sigma_1 + \Delta\sigma_1'$ is weaker. Therefore, $\Delta\sigma_1 + \Delta\sigma_1'$ plays a dominant role at this point, enhancing the PCF scattering potential and causing a decrease in the μ_n after proton irradiation (Figure 7).

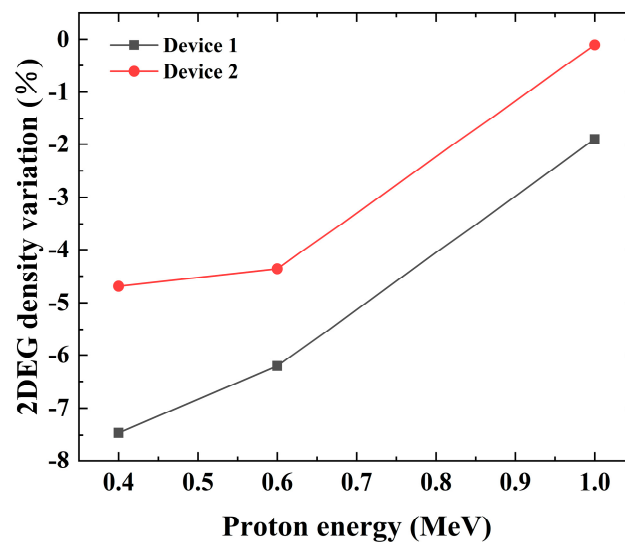


Figure 9. Level of the 2DEG electron density variation after proton irradiation at gate–source voltage $V_{GS} = 0$ V as a function of proton energy.

The action distance of higher energy protons is farther from the barrier layer, and with the proton energy increasing, the non-ionizing energy transferred from the proton to the atom decreases, which causes the degree of displacement damage to decrease [35,36]. This is the reason that the action intensity of higher energy protons on the barrier layer is lower in a certain energy range. It is found from Figure 9 that the amplitude of the n_{2D} variation decreases with increasing proton energy. This indicates that the weakening degree of the tensile strain in region I gradually decreases as the proton energy increases. In other words, the enhancement degree of the tensile strain in region II gradually decreases. Therefore, for devices with the same L_{GD} , the absolute value of $\Delta\sigma_2$ decreases with the increasing proton energy, and the absolute value of $\Delta\sigma_1'$ decreases simultaneously. For Device 1 at a 1 MeV proton irradiation, the influence of $\Delta\sigma_2 + \Delta\sigma_1'$ is weaker than that at a 0.4 MeV proton irradiation. Following Equation (5), the decrease degree of the PCF scattering potential gets lower with the proton energy increasing. As a result, compared with Figure 6c, the increase of μ_n is smaller in Figure 6a. For Device 2 at a 1 MeV proton irradiation, $\Delta\sigma_1 + \Delta\sigma_1'$ plays a dominant role. With the proton energy increasing, the absolute value of $\Delta\sigma_1'$ decreases, and the PCF scattering potential gets lower. This makes the decrease degree of μ_n smaller in Figure 7a, compared with Figure 7c.

4. Conclusions

Based on the PCF scattering theory, the proton irradiation effect on the transport characteristics of AlGaIn/GaN HEMTs is analyzed in terms of the gate–drain distance and proton energy. It is found that the displacement damage caused by protons changes the polarization/strain distribution at the AlGaIn/GaN interface, which affects the 2DEG electron density and intensity of the PCF scattering. Due to the displacement damage, the electron density decreases after proton irradiation. In addition, the decrease degree of the device with a large gate–drain distance is larger. The electron mobility of the device with a large gate–drain distance increases after irradiation due to the weakening of the PCF scattering. For the device with a small gate–drain distance, the electron mobility decreases after irradiation due to the enhancement of the PCF scattering. The change of the electron mobility is the main reason for the difference in the output current. The impact of proton irradiation on the electrical performance gradually decreases with the proton energy increasing. Although the electron density decreases after a 0.4 MeV proton irradiation, the current and low-field electron mobility of the device with a larger gate–drain distance increase. Thus, the proton effect and gate–drain distance can be adjusted appropriately to improve the device performance. Moreover, based on a theoretical model of the PCF scattering, the variation of the strain at the AlGaIn barrier layer is obtained by an analysis of the electrical properties. It is helpful to understand the mechanism of the proton irradiation influence on AlGaIn/GaN HEMTs at the microscopic level. This is beneficial for improving the irradiation resistance of AlGaIn/GaN HEMTs in the field of aerospace.

Author Contributions: Conceptualization, Q.J. and M.Y.; investigation, Q.J. and X.H.; methodology, Q.J. and M.Y.; writing—original draft, Q.J.; writing—review and editing, J.L. and M.Y.; supervision, G.W. and M.Q.; project administration, S.L. All authors have read and agreed to the published version of the manuscript.

Funding: This work was supported by the National Natural Science Foundation of China (Grant No. 61904007).

Data Availability Statement: The data that support the findings are available from the corresponding author upon reasonable request.

Conflicts of Interest: The authors declare that they have no known competing financial interests or personal relationships that could have appeared to influence the work reported in this paper.

References

1. Nguyen, H.Q.; Nguyen, T.; Tanner, P.; Nguyen, T.K.; Faisal, A.R.M.; Fastier-Wooller, J.; Nguyen, T.H.; Phan, H.P.; Nguyen, N.T.; Dao, D.V. Piezotronic effect in a normally off p-GaN/AlGaIn/GaN HEMT toward highly sensitive pressure sensor. *Appl. Phys. Lett.* **2021**, *118*, 242104. [[CrossRef](#)]
2. Narang, K.; Bag, R.K.; Singh, V.K.; Pandey, A.; Saini, S.K.; Khan, R.; Arora, A.; Padmavati, M.V.G.; Tyagi, R.; Singh, R. Improvement in surface morphology and 2DEG properties of AlGaIn/GaN HEMT. *J. Alloys Compd.* **2020**, *815*, 152283. [[CrossRef](#)]
3. Moon, J.S.; Wong, J.; Grabar, B.; Antcliffe, M.; Chen, P.; Arkun, E.; Khalaf, I.; Corrion, A.; Chappell, J.; Venkatesan, N.; et al. 360 GHz f_{MAX} graded-channel AlGaIn/GaN HEMTs for mmW low-noise applications. *IEEE Electron Device Lett.* **2020**, *41*, 1173–1176. [[CrossRef](#)]
4. Pengelly, R.S.; Wood, S.M.; Milligan, J.W.; Sheppard, S.T.; Pribble, W.L. A Review of GaN on SiC High Electron-Mobility Power Transistors and MMICs. *IEEE Trans. Microw. Theory Tech.* **2012**, *60*, 1764–1783. [[CrossRef](#)]
5. Chen, K.J.; Haberlen, O.; Lidow, A.; Tsai, C.L.; Ueda, T.; Uemoto, Y.; Wu, Y. GaN-on-Si power technology: Devices and applications. *IEEE Trans. Electron Devices* **2017**, *64*, 779–795. [[CrossRef](#)]
6. Pearton, S.J.; Ren, F.; Patrick, E.; Law, M.E.; Polyakov, A.Y. Ionizing radiation damage effects on GaN devices. *ECS J. Solid State Sci. Technol.* **2016**, *5*, Q35. [[CrossRef](#)]
7. Ionascut-Nedelcescu, A.; Carlone, C.; Houdayer, A.; von Bardeleben, H.J.; Cantin, J.; Raymond, S. Radiation hardness of gallium nitride. *IEEE Trans. Nucl. Sci.* **2002**, *49*, 2733–2738. [[CrossRef](#)]
8. Abderrahmane, A.; Koide, S.; Tahara, T.; Sato, S.; Ohshima, T.; Okada, H.; Sandhu, A. Effect of proton irradiation on 2DEG in AlGaIn/GaN heterostructures. *J. Phys. Conf. Ser.* **2013**, *433*, 12011. [[CrossRef](#)]
9. Binari, S.C.; Klein, P.B.; Kazior, T.E. Trapping effects in GaN and SiC microwave FETs. *Proc. IEEE* **2002**, *90*, 1048–1058. [[CrossRef](#)]
10. Divay, A.; Latry, O.; Duperrier, C.; Temcamani, F. Ageing of GaN HEMT devices: Which degradation indicators? *J. Semicond.* **2016**, *37*, 14001. [[CrossRef](#)]

11. Hu, X.; Bo, K.C.; Barnaby, H.J.; Fleetwood, D.M.; Schrimpf, R.D.; Lee, S.; Shojah-Ardalan, S.; Wilkins, R.; Mishra, U.K.; Dettmer, R.W. The energy dependence of proton-induced degradation in AlGaIn/GaN high electron mobility transistors. *IEEE Trans. Nucl. Sci.* **2004**, *51*, 293–297. [[CrossRef](#)]
12. Kalavagunta, A.; Silvestri, M.; Beck, M.J.; Dixit, S.K.; Schrimpf, R.D.; Reed, R.A.; Fleetwood, D.M.; Shen, L.; Mishra, U.K. Impact of proton irradiation-induced bulk defects on gate-lag in GaN HEMTs. *IEEE Trans. Nucl. Sci.* **2009**, *56*, 3192–3195. [[CrossRef](#)]
13. Lv, L.; Ma, J.G.; Cao, Y.R.; Zhang, J.C.; Zhang, W.; Li, L.; Xu, S.R.; Ma, X.H.; Ren, X.T.; Hao, Y. Study of proton irradiation effects on AlGaIn/GaN high electron mobility transistors. *Microelectron. Reliab.* **2011**, *51*, 2168–2172. [[CrossRef](#)]
14. Ives, N.E.; Chen, J.; Witulski, A.F.; Schrimpf, R.D.; Fleetwood, D.M.; Bruce, R.W.; McCurdy, M.W.; Zhang, E.X.; Massengill, L.W. Effects of proton-induced displacement damage on gallium nitride HEMTs in RF power amplifier applications. *IEEE Trans. Nucl. Sci.* **2015**, *62*, 2417–2422. [[CrossRef](#)]
15. Kim, D.S.; Lee, J.H.; Kim, J.G.; Yoon, Y.J.; Lee, J.S.; Lee, J.H. Anomalous DC characteristics of AlGaIn/GaN HEMTs depending on proton irradiation energies. *ECS J. Solid State Sci. Technol.* **2020**, *9*, 65005. [[CrossRef](#)]
16. Tang, J.; Liu, G.; Zhao, G.; Xing, S.; Malik, S.A. Effect of proton irradiation on the mobility of two-dimensional electron in AlGaIn/AlN/GaN high electron mobility transistors at low temperature. *J. Vac. Sci. Technol. B* **2020**, *38*, 23202. [[CrossRef](#)]
17. Tang, J.J.; Liu, G.P.; Song, J.Y.; Zhao, G.J.; Yang, J.H. Analysis of the decrease of two-dimensional electron gas concentration in GaN-based HEMT caused by proton irradiation. *Chin. Phys. B* **2021**, *30*, 27303. [[CrossRef](#)]
18. Ambacher, O.; Smart, J.; Shealy, J.R.; Weimann, N.G.; Chu, K.; Murphy, M.; Schaff, W.J.; Eastman, L.F.; Dimitrov, R.; Wittmer, L.; et al. Two-dimensional electron gases induced by spontaneous and piezoelectric polarization charges in N- and Ga-face AlGaIn/GaN heterostructures. *J. Appl. Phys.* **1999**, *85*, 3222–3233. [[CrossRef](#)]
19. Yuan, L.; Chen, H.; Chen, K.J. Normally off AlGaIn/GaN metal–2DEG tunnel-junction field-effect transistors. *IEEE Electron Device Lett.* **2011**, *32*, 303–305. [[CrossRef](#)]
20. Cui, P.; Liu, H.; Lin, W.; Lin, Z.; Cheng, A.; Yang, M.; Liu, Y.; Fu, C.; Lv, Y.; Luan, C. Influence of different gate biases and gate lengths on parasitic source access resistance in AlGaIn/GaN heterostructure FETs. *IEEE Trans. Electron Devices* **2017**, *64*, 1038–1044. [[CrossRef](#)]
21. Lv, Y.; Lin, Z.; Meng, L.; Luan, C.; Cao, Z.; Yu, Y.; Feng, Z.; Wang, Z. Influence of the ratio of gate length to drain-to-source distance on the electron mobility in AlGaIn/AlN/GaN heterostructure field-effect transistors. *Nanoscale Res. Lett.* **2012**, *7*, 434. [[CrossRef](#)]
22. Liu, Y.; Lin, Z.J.; Yang, M.; Luan, C.B.; Wang, Y.T.; Lv, Y.J.; Feng, Z.H. Effect of polarization Coulomb field scattering on low temperature electron mobility in strained AlGaIn/AlN/GaN heterostructure field-effect transistors. *Mod. Phys. Lett. B* **2016**, *30*, 1650411. [[CrossRef](#)]
23. Yang, M.; Ji, Q.; Su, X.; Zhang, W.; Wang, Y.; Wang, L.; Hu, X.; Yuan, Q.; Feng, P.; Liu, Y. Study on the electron mobility related with ohmic contact width in AlGaIn/GaN HEMTs. *Mod. Phys. Lett. B* **2020**, *34*, 2150008. [[CrossRef](#)]
24. Zhao, J.; Lin, Z.; Corrigan, T.D.; Wang, Z.; You, Z.; Wang, Z. Electron mobility related to scattering caused by the strain variation of AlGaIn barrier layer in strained AlGaIn/GaN heterostructures. *Appl. Phys. Lett.* **2007**, *91*, 173507. [[CrossRef](#)]
25. Dongmin, K.; Hyungtak, K. Energy-Dependent Degradation Characteristics of AlGaIn/GaN MISHEMTs with 1, 1.5, and 2 MeV Proton Irradiation. *ECS J. Solid State Sci. Technol.* **2018**, *7*, Q159–Q163.
26. Yang, M.; Ji, Q.; Wang, Y.; Hu, X.; Yuan, Q.; Liu, X.; He, J.; Wang, R.; Zhou, L.; Xiao, J.; et al. Drain Schottky contact influence on low-field transport characteristic of AlGaIn/GaN heterostructure field-effect transistors. *Appl. Phys. A* **2022**, *128*, 460. [[CrossRef](#)]
27. Lv, Y.; Lin, Z.; Zhang, Y.; Meng, L.; Luan, C.; Cao, Z.; Chen, H.; Wang, Z. Polarization Coulomb field scattering in AlGaIn/AlN/GaN heterostructure field-effect transistors. *Appl. Phys. Lett.* **2011**, *98*, 123512. [[CrossRef](#)]
28. Yang, M.; Lv, Y.; Cui, P.; Liu, Y.; Fu, C.; Lin, Z. Determination of the polarization and strain distribution in AlGaIn/GaN heterostructure field-effect transistors. *J. Phys. Chem. Solids* **2018**, *123*, 223–227. [[CrossRef](#)]
29. Luan, C.; Lin, Z.; Lv, Y.; Zhao, J.; Wang, Y.; Chen, H.; Wang, Z. Theoretical model of the polarization Coulomb field scattering in strained AlGaIn/AlN/GaN heterostructure field-effect transistors. *J. Appl. Phys.* **2014**, *116*, 44507. [[CrossRef](#)]
30. Yang, M.; Lv, Y.; Feng, Z.; Lin, W.; Cui, P.; Liu, Y.; Fu, C.; Lin, Z. Study of source access resistance at direct current quiescent points for AlGaIn/GaN heterostructure field-effect transistors. *J. Appl. Phys.* **2016**, *119*, 224501. [[CrossRef](#)]
31. Gurusinghe, M.N.; Davidsson, S.K.; Andersson, T.G. Two-dimensional electron mobility limitation mechanisms in Al_xGa_{1-x}N/GaN heterostructures. *Phys. Rev. B* **2005**, *72*, 45316. [[CrossRef](#)]
32. Yang, M.; Lin, Z.; Zhao, J.; Cui, P.; Fu, C.; Lv, Y.; Feng, Z. Effect of Polarization Coulomb Field Scattering on Parasitic Source Access Resistance and Extrinsic Transconductance in AlGaIn/GaN Heterostructure FETs. *IEEE Trans. Electron Devices* **2016**, *63*, 1471–1477. [[CrossRef](#)]
33. Ibbetson, J.P.; Fini, P.T.; Ness, K.D.; DenBaars, S.P.; Speck, J.S.; Mishra, U.K. Polarization effects, surface states, and the source of electrons in AlGaIn/GaN heterostructure field effect transistors. *Appl. Phys. Lett.* **2000**, *77*, 250–252. [[CrossRef](#)]
34. Goyal, N.; Iñiguez, B.; Fjeldly, T.A. Analytical modeling of bare surface barrier height and charge density in AlGaIn/GaN heterostructures. *Appl. Phys. Lett.* **2012**, *101*, 103505. [[CrossRef](#)]

35. Lv, L.; Zhang, J.C.; Li, L.; Ma, X.H.; Cao, Y.R.; Hao, Y. Effects of 3 MeV proton irradiations on AlGaN/GaN high electron mobility transistors. *Acta Phys. Sinica* **2012**, *61*, 57202.
36. Sonia, G.; Richter, E.; Lossy, R.; Mai, M.; Schmidt, J.; Weyers, M.; Tränkle, G.; Denker, A.; Opitz-Coutureau, J.; Pensl, G.; et al. High and low energy proton irradiation effects on AlGaN/GaN HFETs. *Phys. Stat. Sol. C* **2006**, *3*, 2338–2341. [[CrossRef](#)]

Disclaimer/Publisher’s Note: The statements, opinions and data contained in all publications are solely those of the individual author(s) and contributor(s) and not of MDPI and/or the editor(s). MDPI and/or the editor(s) disclaim responsibility for any injury to people or property resulting from any ideas, methods, instructions or products referred to in the content.